Electronic Supplementary Information (ESI)

In-situ growth of $Cu(OH)_2$@FeOOH nanotubes arrays on catalytically deposited Cu current collector patterns for high-performance flexible in-plane micro-size energy storage devices

Jin-Qi Xie,[ab] Ya-Qiang Ji,[a] Jia-Hui Kang,[a] Jia-Li Sheng,[a] Da-Sha Mao,[ab] Xian-Zhu Fu,[*ac] Rong Sun[a] and Ching-Ping Wong[de]

[a] Shenzhen Institutes of Advanced Technology, Chinese Academy of Sciences, Shenzhen 518055, China.

[b] Shenzhen College of Advanced Technology, University of Chinese Academy of Sciences, Beijing, China.

[c] College of Materials Science and Engineering, Shenzhen University, Shenzhen 518055, China.

[d] Department of Electronics Engineering, The Chinese University of Hong Kong, Hong Kong, China.

[e] School of Materials Science and Engineering, Georgia Institute of Technology, Atlanta, GA 30332, United States.

*E-mail: xz.fu@szu.edu.cn

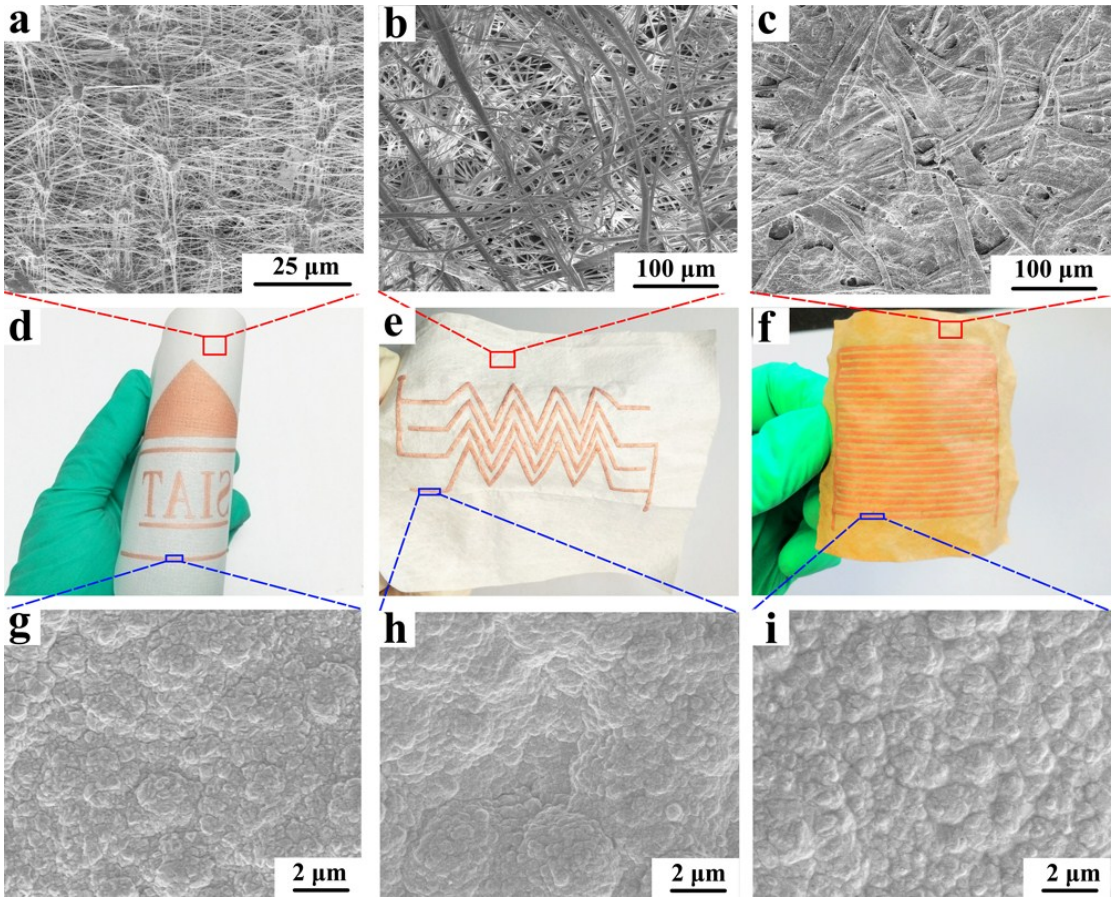

Fig. S1 Surface SEM images of (a) PTFE, (b) cotton cloth and (c) waste paper. Digital photos of electroless deposited copper patterns on (d) PTFE, (e) cotton cloth and (f) waste paper. Surface SEM images of the electroless deposited copper on (g) PTFE, (h) cotton cloth and (i) waste paper.

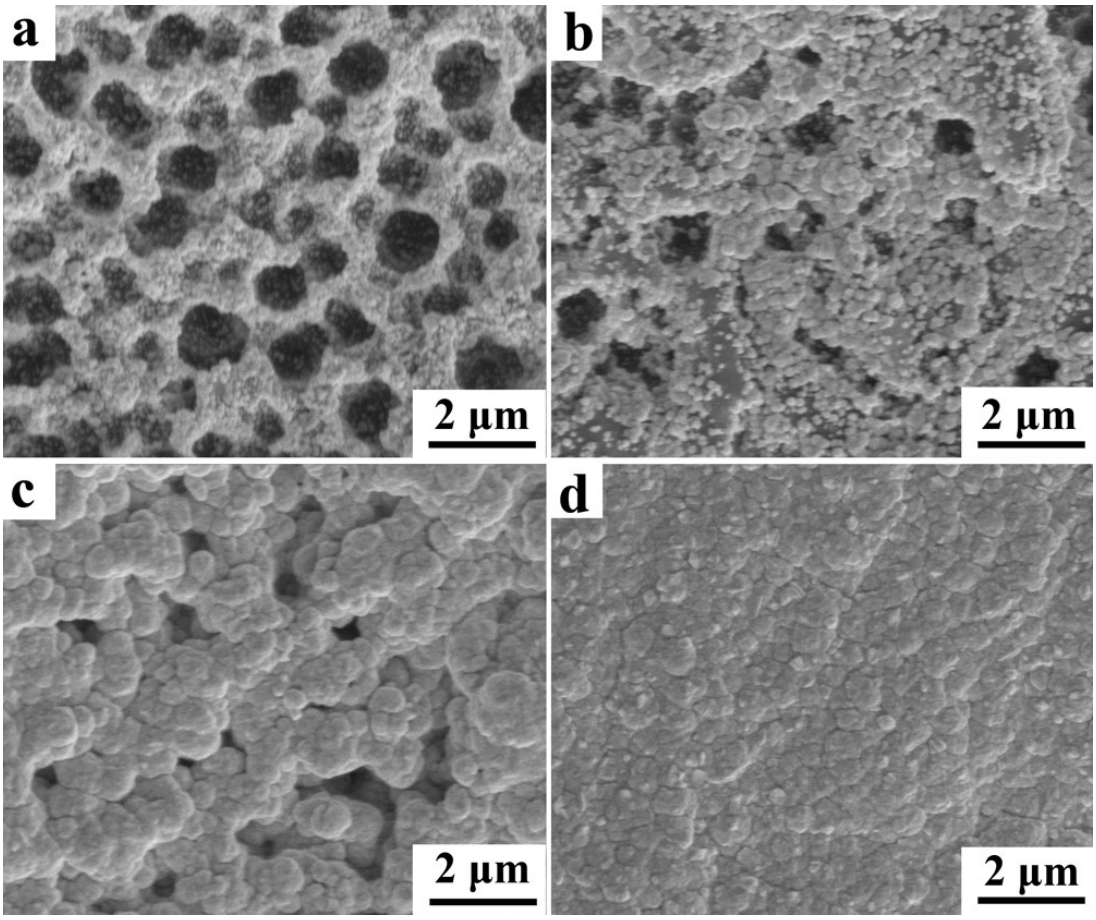

Fig. S2 Surface SEM images of Cu coatings on PI (filled in epoxy resin) at ECD time of (a) 5 min, (b) 10 min, (c) 15 min and (d) 30 min.

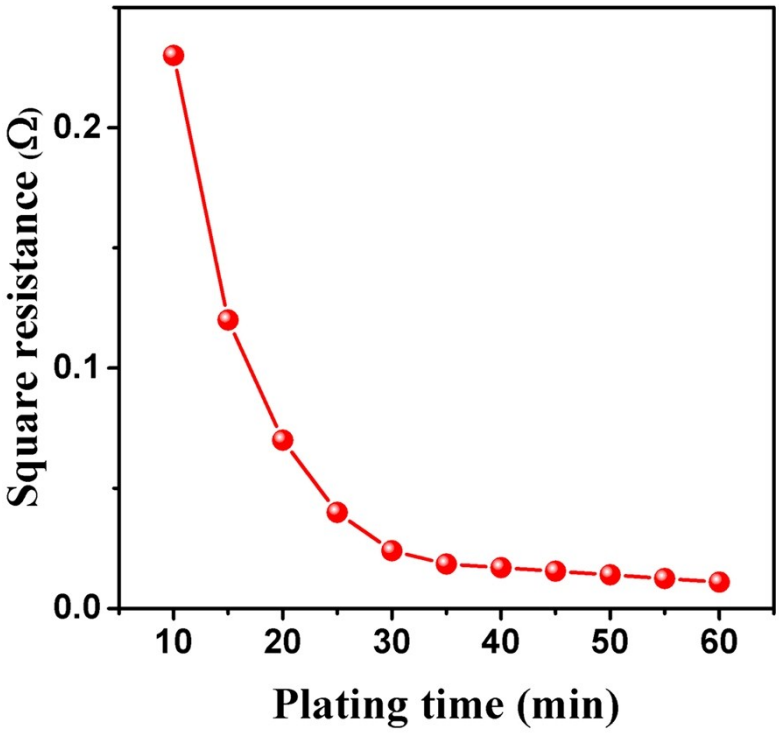

Fig. S3 The variation of the surface resistivity of Cu coating with ECD time.

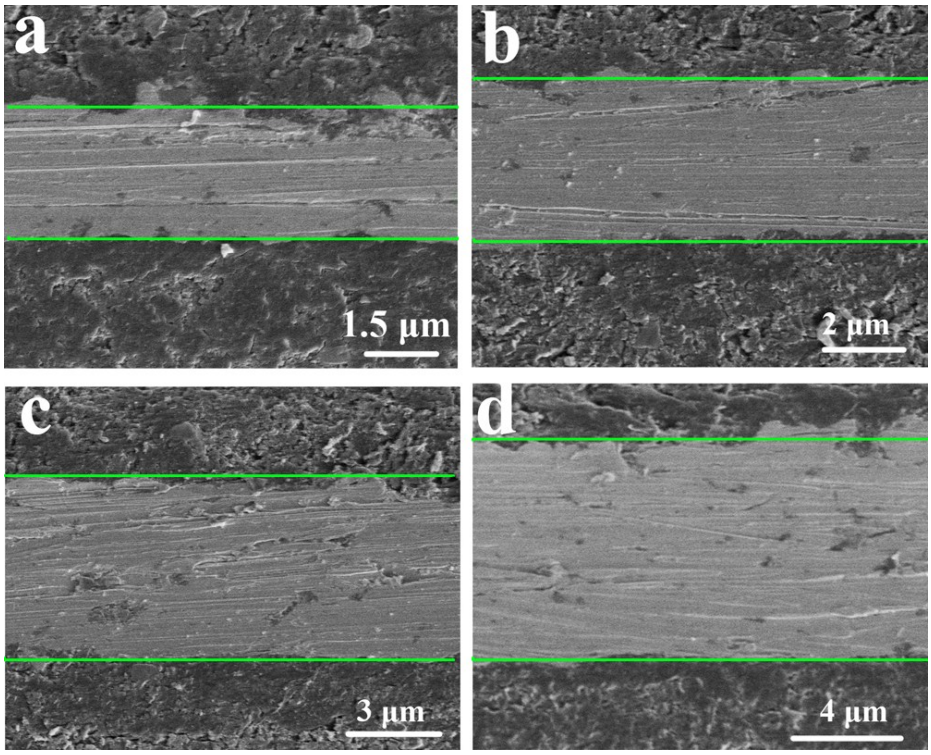

Fig. S4 Cross-sectional SEM images of Cu coatings on PI (filled in epoxy resin) at ECD time of (a) 1h, (b) 1.5h, (c) 3h and (d) 6h.

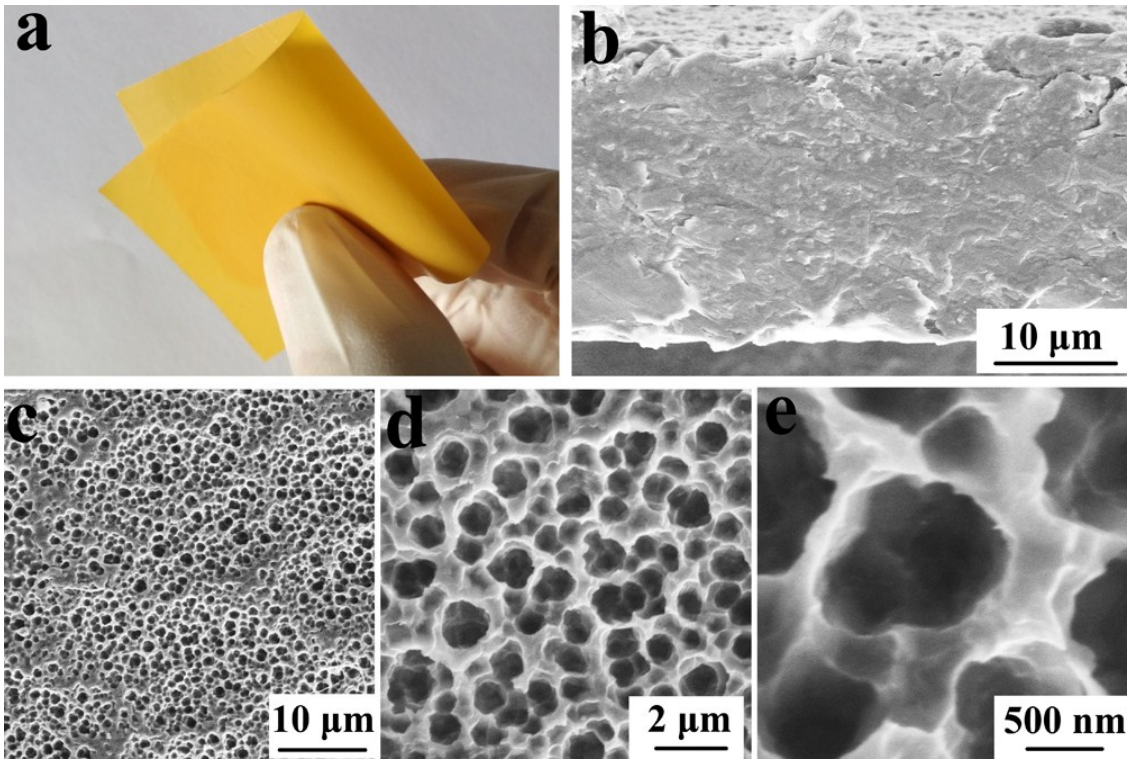

Fig. S5 (a) digital image, (b) Cross-sectional SEM image and (c-e) surface SEM images of the PI substrate.

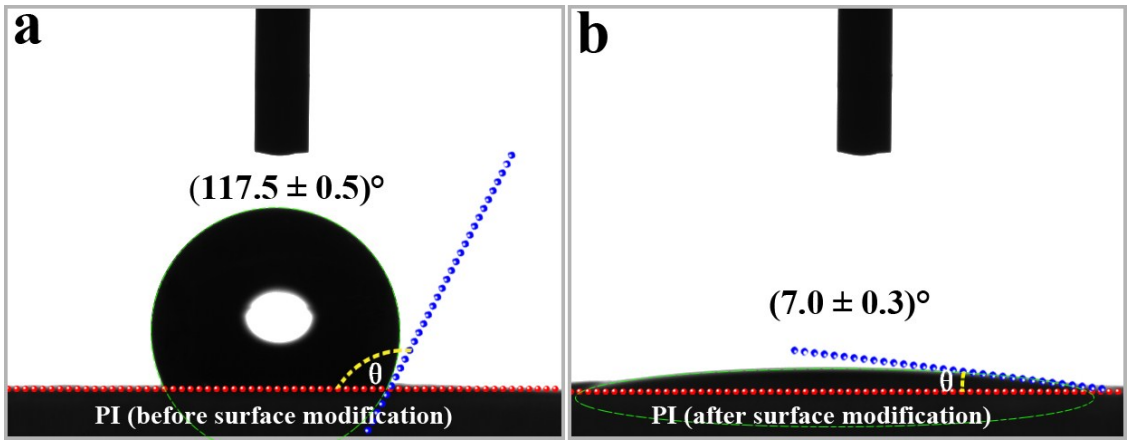

Fig. S6 Contact angles between water and PI substrates (a) before and (b) after surface modification.

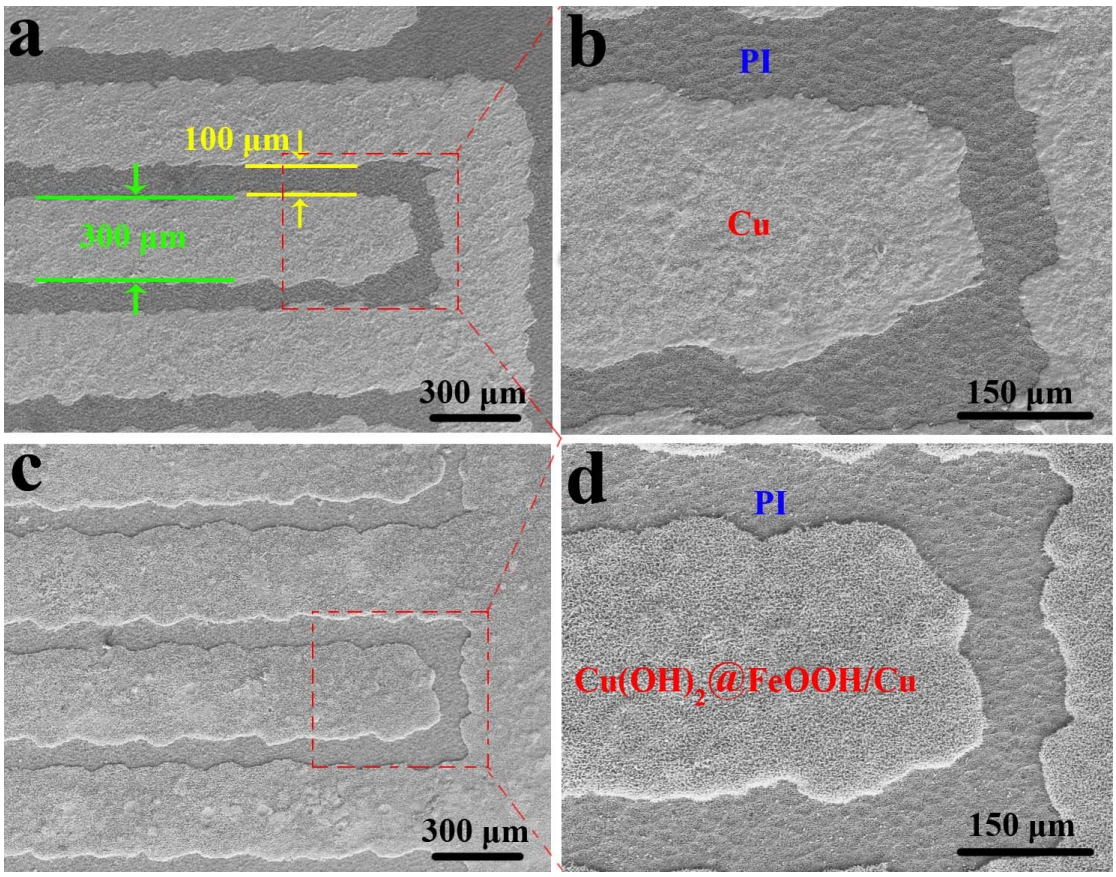

Fig. S7 Surface SEM images of interdigital electrodes: (a) Cu/PI and (b) $Cu(OH)_2$@FeOOH NTs array /Cu/PI.

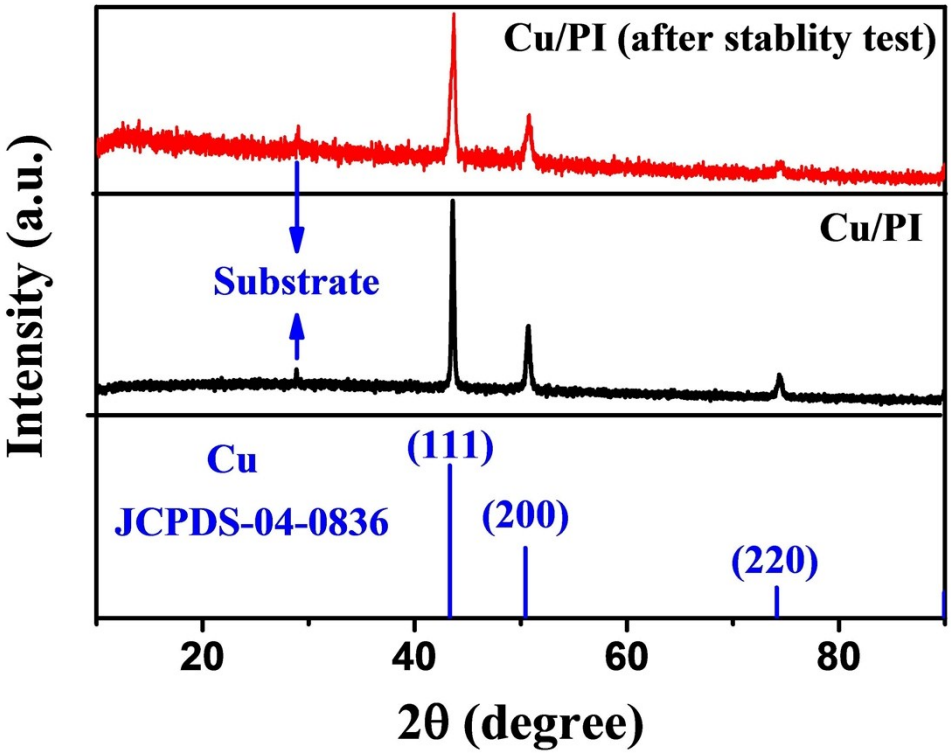

Fig. S8 XRD patterns of the electroless deposited cooper before and after stability test.

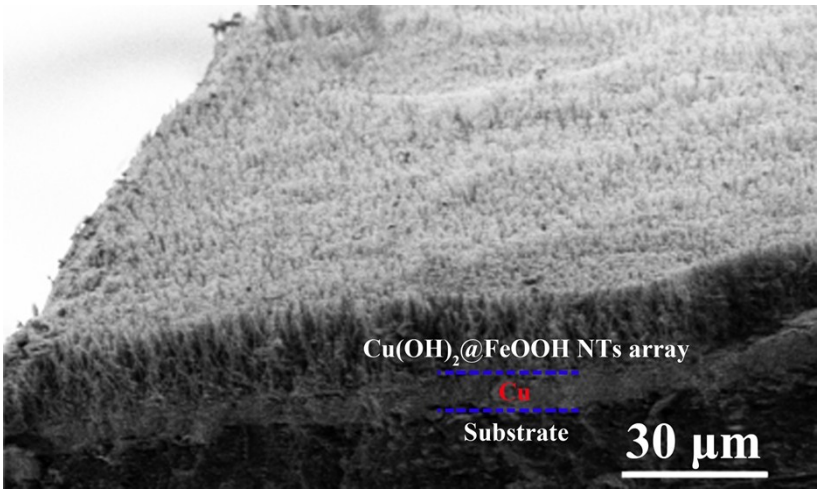

Fig. S9 Cross-sectional SEM image of the $Cu(OH)_2$@FeOOH NTs array/Cu electrode.

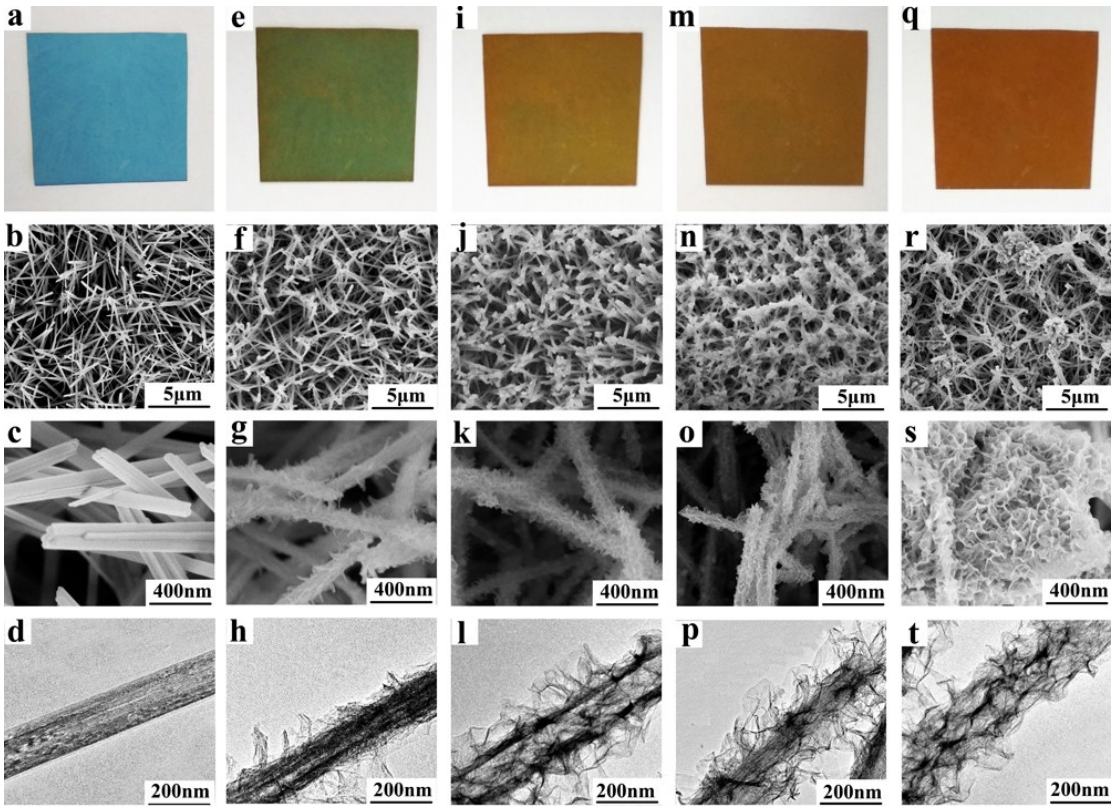

Fig. S10 (a) Digital photo, (c-d) SEM images and (d) TEM image of $Cu(OH)_2$. (e) Digital photo, (f-g) SEM images and (h) TEM image of $Cu(OH)_2$@FeOOH-1. (i) Digital photo, (j-k) SEM images and (l) TEM image of $Cu(OH)_2$@FeOOH-2. (m) Digital photo, (n-o) SEM images and (p) TEM image of $Cu(OH)_2$@FeOOH-3. (q) Digital photo, (r-s) SEM images and (t) TEM image of $Cu(OH)_2$@FeOOH-4.

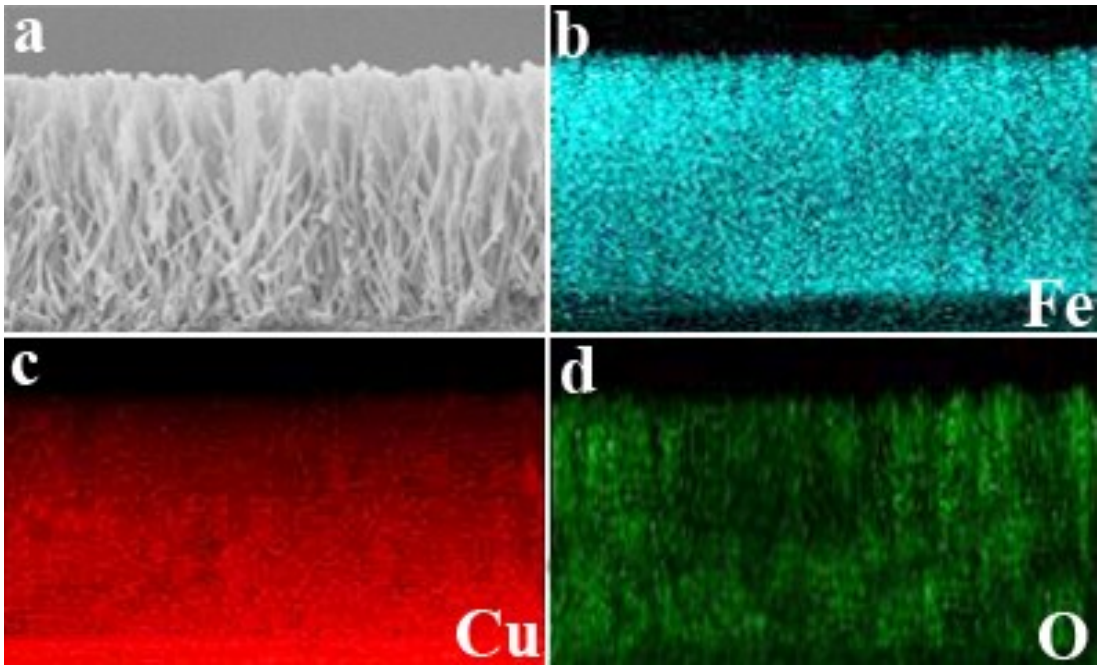

Fig. S11 (a) Cross-sectional SEM image and (b-d) SEM-EDS mapping of the Cu(OH)2@FeOOH NTs array.

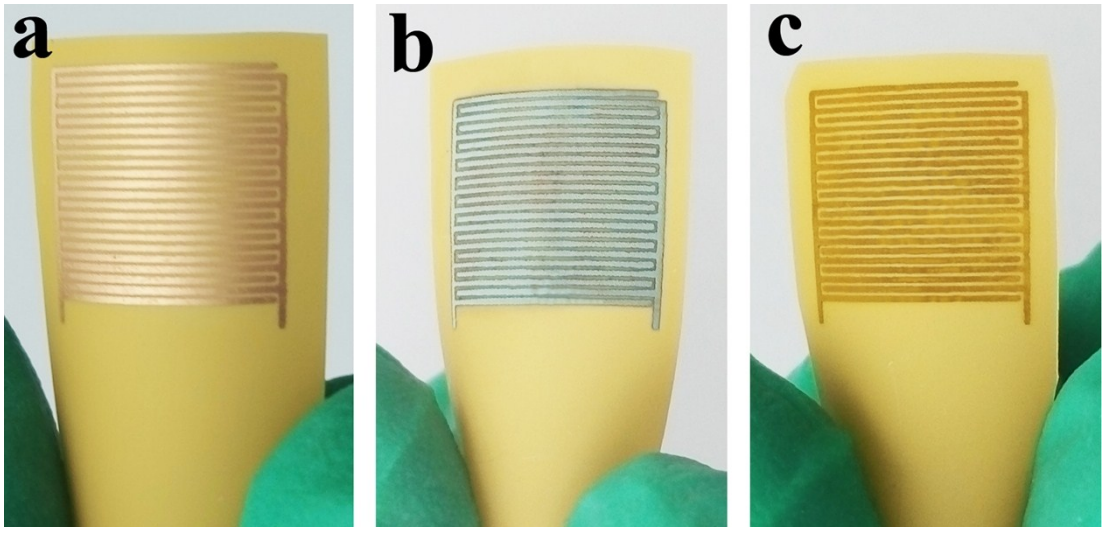

Fig. S12 Digital images of the as-fabricated interdigitated electrodes: (a) Cu/PI, (b) $Cu(OH)_2$ NWs array/Cu/PI and (c) $Cu(OH)_2$@FeOOH NTs array/Cu/PI.

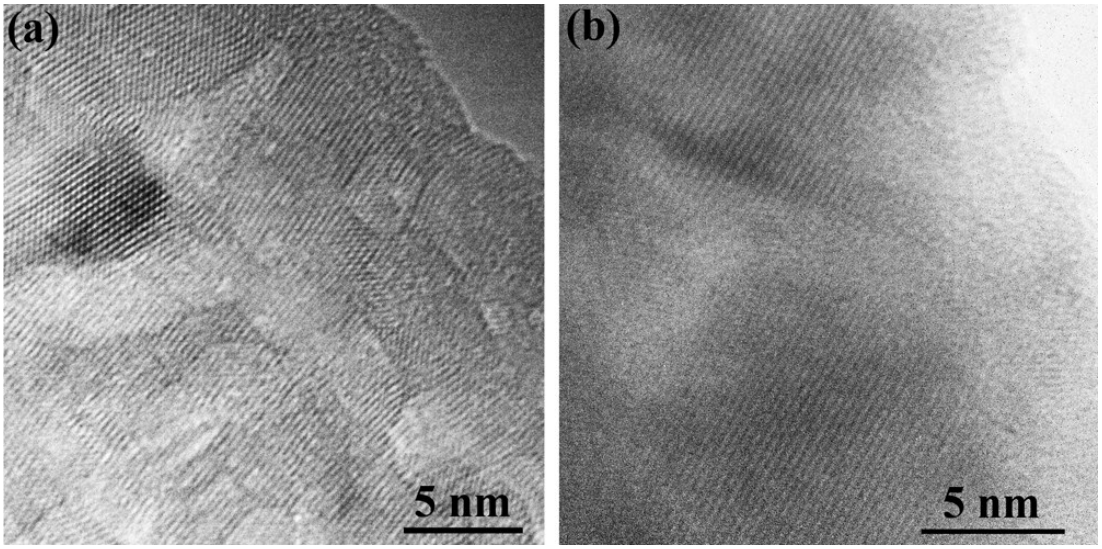

Fig. S13 HRTEM images of (a) $Cu(OH)_2$ NWs and (b) FeOOH nanosheet.

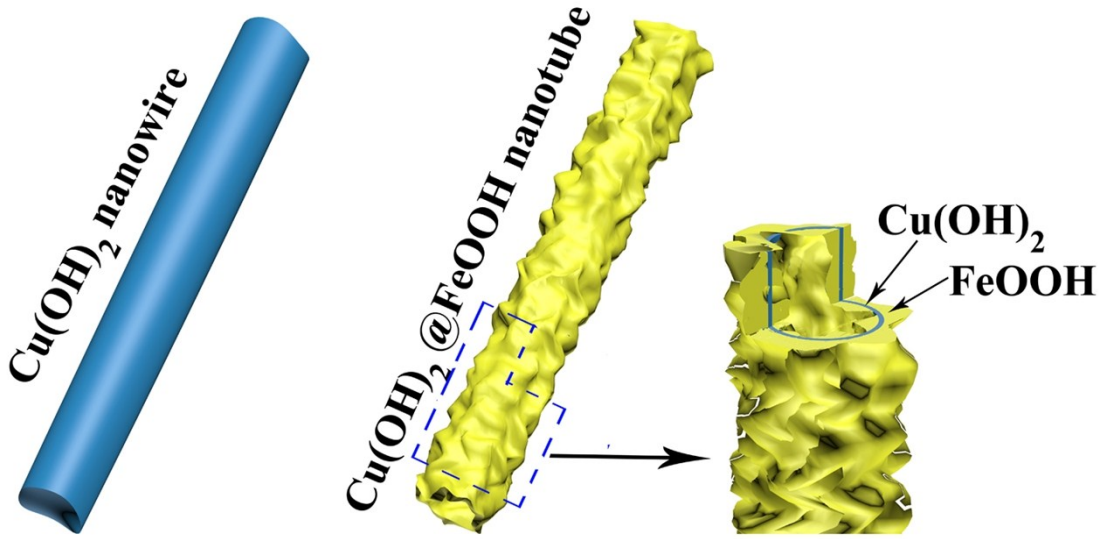

Fig. S14 Structure illustration of the $Cu(OH)_2$ NWs and $Cu(OH)_2$@FeOOH NTs.

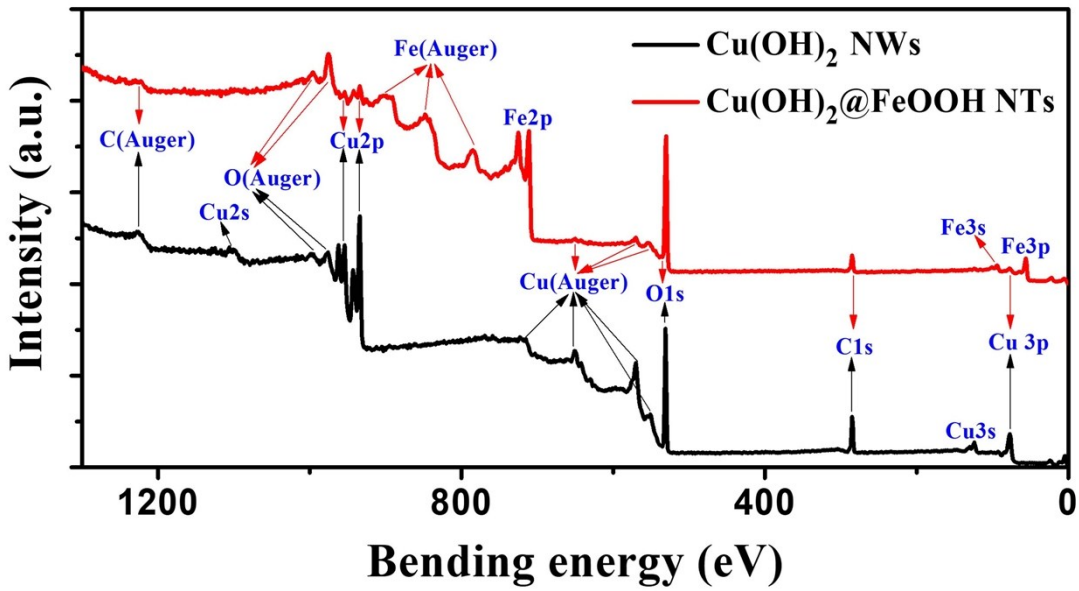

Fig. S15 The survey XPS spectra of the $Cu(OH)_2$ NWs and the $Cu(OH)_2$@FeOOH NTs.

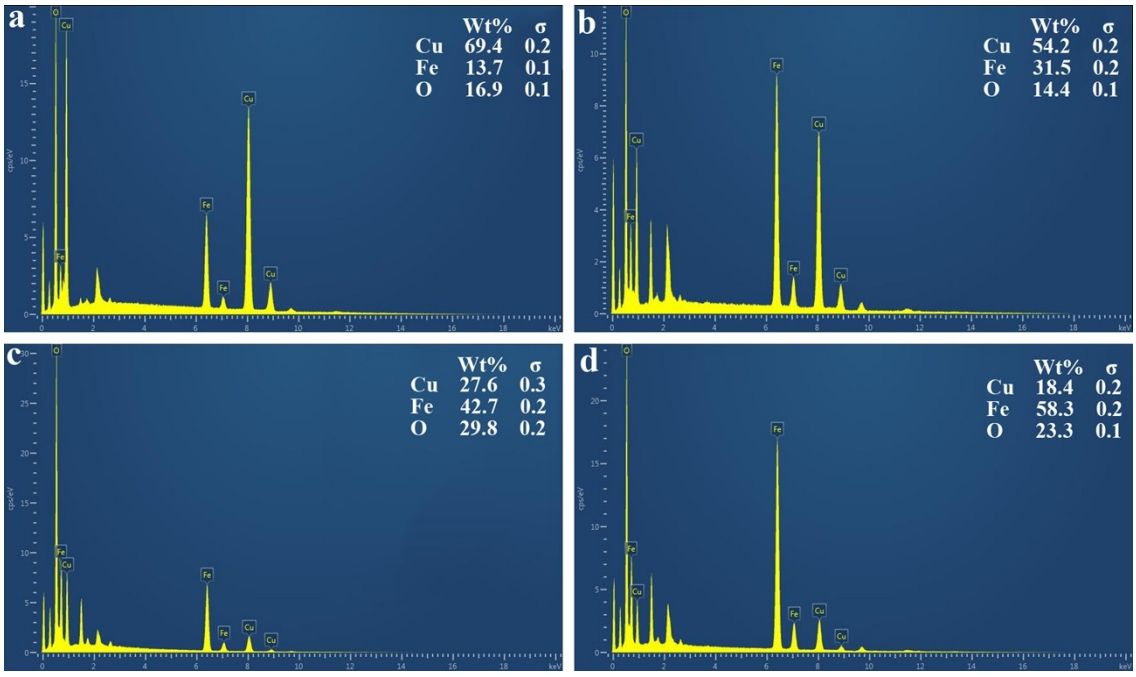

Fig. S16 EDS spectra of (a) $Cu(OH)_2$@FeOOH-1 (b) $Cu(OH)_2$@FeOOH-2, (c) $Cu(OH)_2$@FeOOH-3 and (d) $Cu(OH)_2$@FeOOH-4.

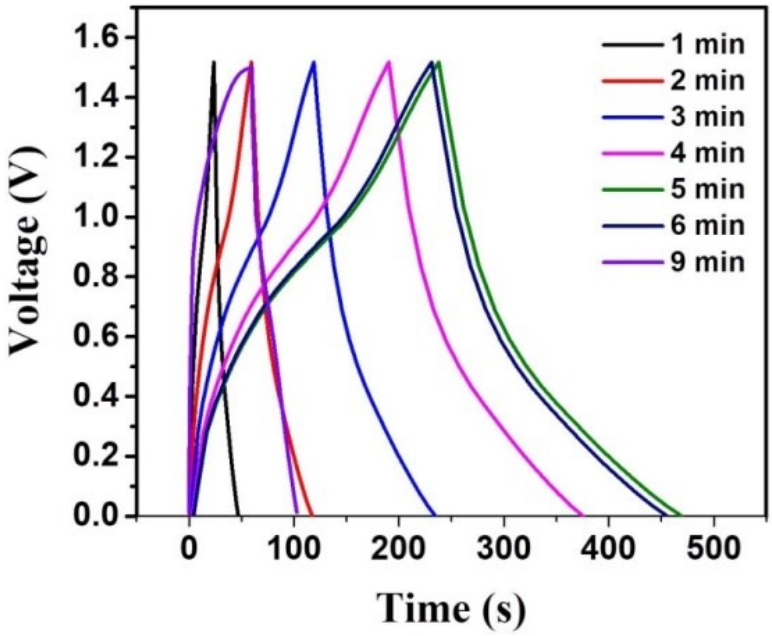

Fig. S17 GCD curves of MSCs fabricated by Cu electrodes immersed in NaOH&$(NH_4)_2SO_3$ aqueous solution with different immersing time at 0.2 mA cm^{-2}.

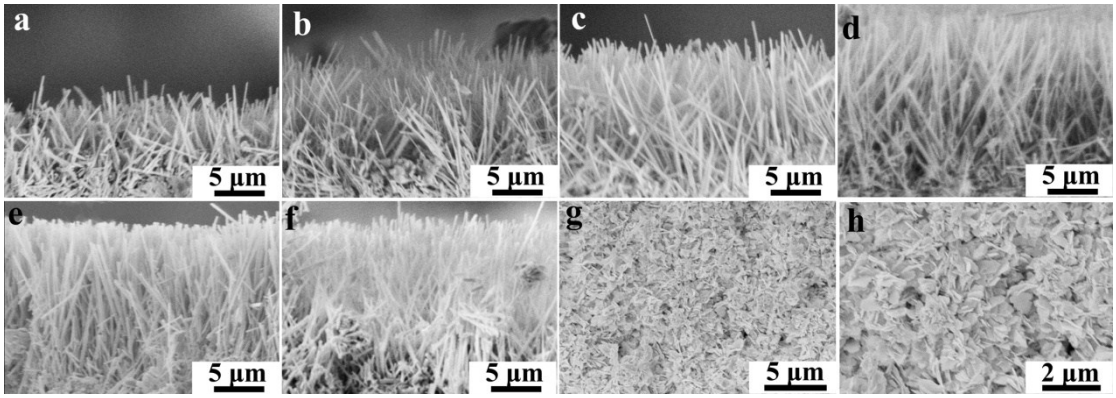

Fig. S18 Sectional SEM images of $Cu(OH)_2$ NWs array with immersing time at (a) 1 minute, (b) 2 minutes, (c) 3 minutes, (d) 4 minutes, (e) 5 minutes and (f) 6 minutes. (g, h) Surface SEM images of the structure with immersing time at 9 minutes.

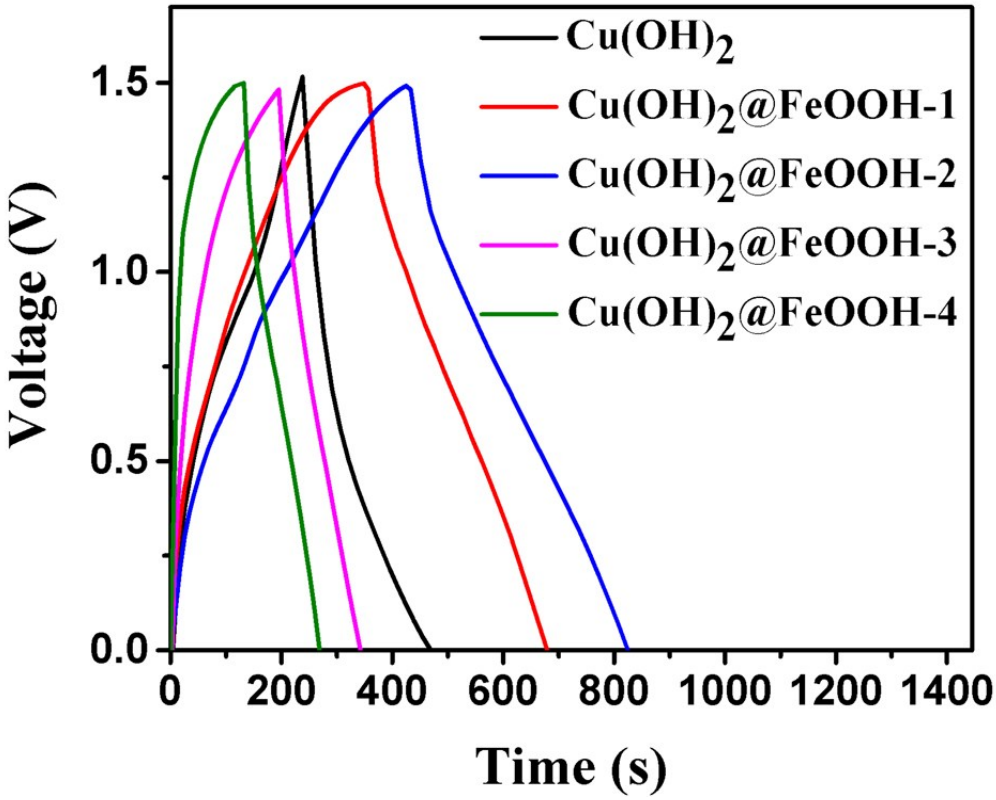

Fig. S19 GCD curves of MSCs fabricated by $Cu(OH)_2$/Cu electrodes immersed in $FeCl_2$ aqueous solution with different immersing time at 0.2 mA cm^{-2}.

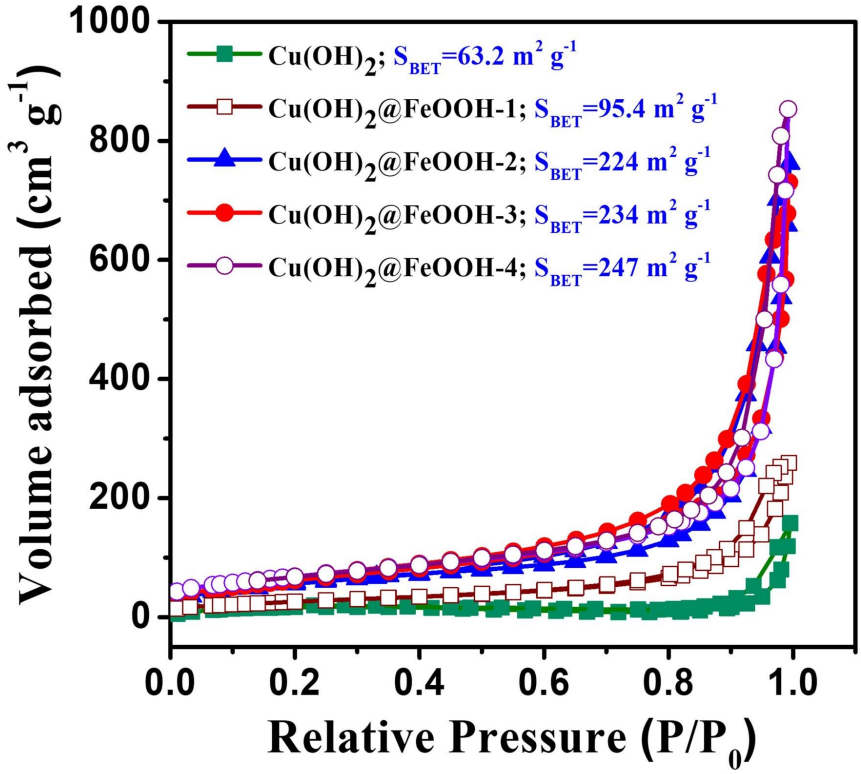

Fig. S20 The N_2 adsorption and desorption isotherms of $Cu(OH)_2$, $Cu(OH)_2$@FeOOH-1, $Cu(OH)_2$@FeOOH-2, $Cu(OH)_2$@FeOOH-3 and $Cu(OH)_2$@FeOOH-4.

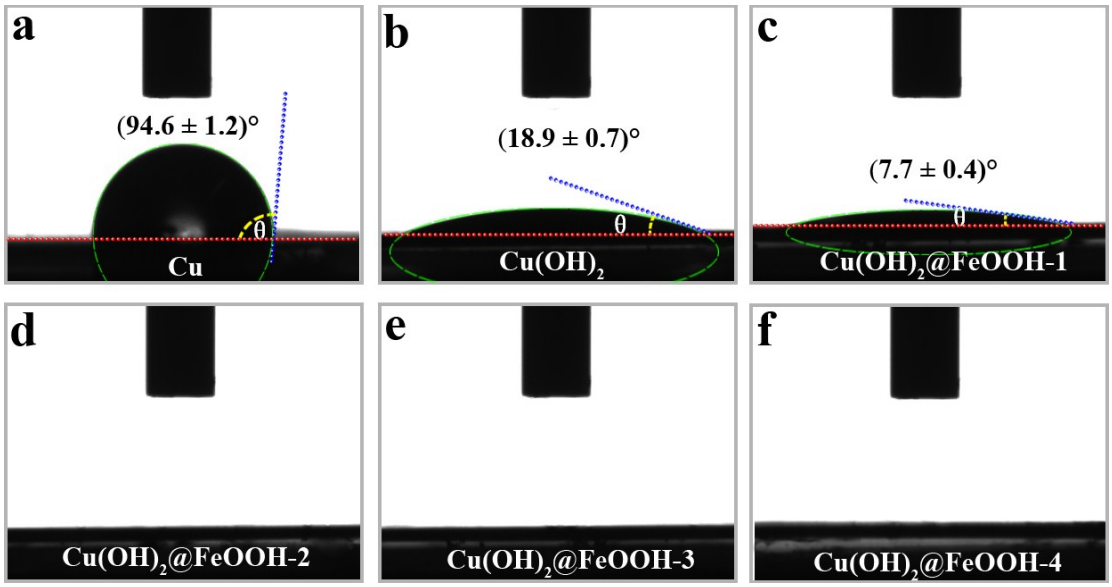

Fig. S21 Contact angles between the electrolyte and (a) Cu, (b) $Cu(OH)_2$, (c) $Cu(OH)_2$@FeOOH-1, (d) $Cu(OH)_2$@FeOOH-2, (e) $Cu(OH)_2$@FeOOH-3 and (f) $Cu(OH)_2$@FeOOH-4.

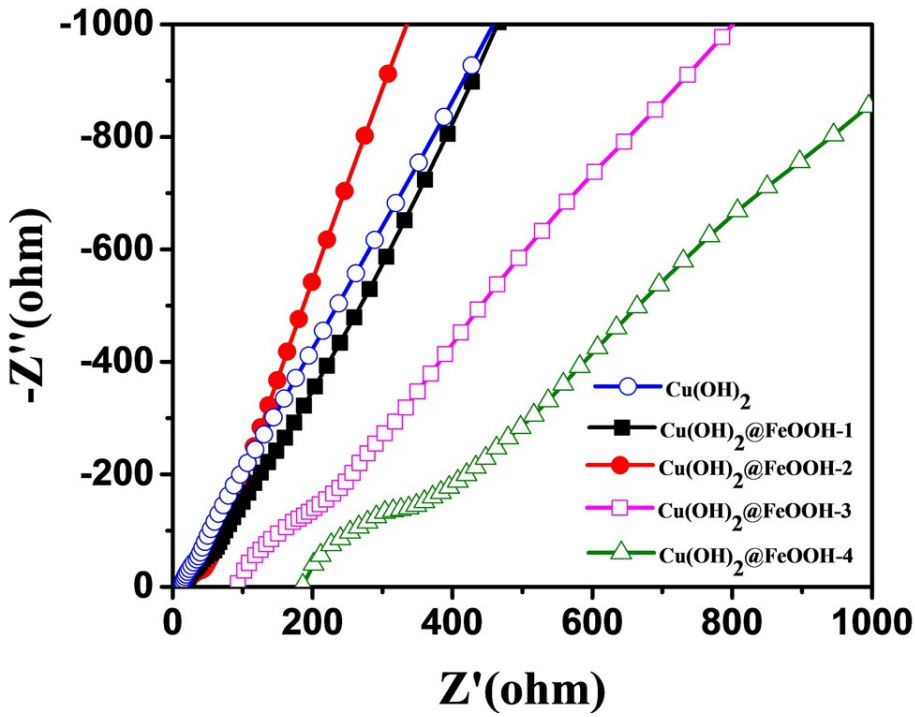

Fig. S22 EIS curves of MSCs fabricated by different electrodes.

Table S1. Comparison of current collector, patterning technology, active materials, synthesis method and electrochemical performances of various MSCs.

Current collector	**Patterning technique**	**active materials**	**Synthesis/loading mehod**	**Areal capacitance (mF cm-2)**	**Areal energy density (μWh cm-2)**
3D graphene [1]	Laser cutting and milling	3D graphene	Chemical vapor deposition	~10 (5mVs^{-1})	0.38
Au/Ag ink [2]	Ink-jet printing; magnetron sputtering	Ni@MnO2 nanocoral	Electrodeposition	52.7 (5mVs^{-1}) 43.7 (0.54mA cm^{-2})	3.88*
Carbon [3]	Spin coating; photolithography	MoS2 nanosheets @rGO-CNTs	Hydrothermal synthesis/spin coating;	13.7 (0.1 mA cm^{-2})	1.9
Au [4]	Photolithography and magnetron sputtering	PPy film	Electrodeposition	47.42 (0.1mA cm^{-2})	4.0
Au[5]	Magnetron sputtering via a printed mask	MnO2	Electrodeposition	11.9 (0.5mA cm^{-2})	1.05*
Au[6]	Magnetron sputtering Laser etching	rGO-PEDOT/PSS	Solution-based reaction /bar-coating	84.7 (T^a=58 μm; 5mVs^{-1}) 26.7 (T=12 μm; 5mVs^{-1})	13.1
Ag nanowires ink [7]	Ink-jet printing;	Active carbon/carbon nanotubes	Ink-jet printing	~20 (0.2mA cm^{-2})*	11.1*
PPy NWs [8]	Electrodeposition on customized fluorine-doped tin oxide pattern	PPy NWs	Electrodeposition	~11 (0.2mA cm^{-2})	0.38*
Ni [9]	Electroless Ni deposition via a laser-etched mask (Kapton tape)	rGO	Hydrothermal synthesis/spontaneous assembly	8.19 (10 5mVs^{-1}) 5.75 (0.1m A cm^{-2})	0.51*

3D porous graphene [10]	Laser etching	3D porous graphene	freeze-casting assisted filtration assembly method	2.47 (5mVs^{-1})	0.22
Ni [11]	Screen printing, Electroless Ni deposition and Electroplating Ni	MnO2; PPy	electrodeposition	25.8 (0.3m A cm^{-2})	8.05
rGO/Au [12]	Laser writing on GO/HAuCl4 mixture	rGO/Au	Laser writing on GO/HAuCl4 mixture	3.84 (1V s^{-1})	0.53
MXenes (Ti3C2Tx) [13]	Patterned by a 3D-printed stamp.	MXenes	Solution-based reaction	15.25 (0.025 mA cm^{-2})* 12.5 (0.8 m A cm^{-2})*	0.63
Ti/Au [14]	vacuum evaporation with a shadow mask	VOx/rGO; graphene-vanadium nitride quantum dots/rGO	Inks preparation: GO (Hummer's method); V_2O_5 (hydrothermal synthesis); Graphene-vanadium nitride quantum dots (hydrothermal synthesis). Loading method: 3D printing.	207.9 (T=412 μm)	73.9
Cu (This work)	Screening printing and Electroless cooper deposition	CuOH@FeOOH nanotubes	In situ conversion (solution immersion at room temperature)	58.0 (0.1 mA cm^{-2})	18.07

[a] T: thickness of the active material.

* Calculated based on the dimensions given in reference if specific results were not given in literature.

Calculations:

The calculations of the areal capacitance (C_A) and the volumetric capacitance (C_V) based on discharging profiles were derived by the following equations:

$$C_{device} = \frac{It}{U} \tag{S1}$$

$$C_A = \frac{C_{device}}{A} \tag{S2}$$

$$C_V = \frac{C_A}{d} \tag{S3}$$

where v is the scanning rate, U is the voltage window, I is the discharging current, t is the discharging time and A is the area of the MSC, d is the thickness of the device including thickness of both the active materials and the current collector.

The areal energy density (E_A) and power density (P_A) of the MSC were respectively calculated by the following equations:

$$E_A = \frac{1}{2} \times C_A \times \frac{U^2}{3600} \tag{S4}$$

$$E_V = \frac{1}{2} \times C_V \times \frac{U^2}{3600} \tag{S5}$$

$$P_A = \frac{3600 \times E_A}{t} \tag{S6}$$

$$P_V = \frac{3600 \times E_V}{t} \tag{S7}$$

References

1. L. Zhang, D. DeArmond, N. T. Alvarez, R. Malik, N. Oslin, C. McConnell, P. K. Adusei, Y. Y. Hsieh and V. Shanov, *Small*, 2017, **13**.
2. Y. J. Lin, Y. Gao and Z. Y. Fan, *Adv Mater*, 2017, **29**.
3. W. Yang, L. He, X. C. Tian, M. Y. Yan, H. Yuan, X. B. Liao, J. S. Meng, Z. M. Hao and L. Q. Mai, *Small*, 2017, **13**.
4. L. Li, C. W. Fu, Z. Lou, S. Chen, W. Han, K. Jiang, D. Chen and G. Z. Shen, *Nano Energy*, 2017, **41**, 261-268.
5. H. B. Hu, Z. B. Pei, H. J. Fan and C. H. Ye, *Small*, 2016, **12**, 3059-3069.

6. Y. Q. Liu, B. Weng, Q. Xu, Y. Y. Hou, C. Zhao, S. Beirne, K. W. Shu, R. Jalili, G. G. Wallace, J. M. Razal and J. Chen, *Adv Mater Technol-Us*, 2016, **1**.
7. K. H. Choi, J. Yoo, C. K. Lee and S. Y. Lee, *Energ Environ Sci*, 2016, **9**, 2812-2821.
8. M. S. Zhu, Y. Huang, Y. Huang, H. F. Li, Z. F. Wang, Z. X. Pei, Q. Xue, H. Y. Geng and C. Y. Zhi, *Adv Mater*, 2017, **29**.
9. X. Pu, M. M. Liu, L. X. Li, S. C. Han, X. L. Li, C. Y. Jiang, C. H. Du, J. J. Luo, W. G. Hu and Z. L. Wang, *Adv Energy Mater*, 2016, **6**.
10. Y. L. Shao, J. M. Li, Y. G. Li, H. Z. Wang, Q. H. Zhang and R. B. Kaner, *Mater Horiz*, 2017, **4**, 1145-1150.
11. R. S. Guo, J. T. Chen, B. J. Yang, L. Y. Liu, L. J. Su, B. S. Shen and X. B. Yan, *Adv Funct Mater*, 2017, **27**.
12. R. Z. Li, R. Peng, K. D. Kihm, S. Bai, D. Bridges, U. Tumuluri, Z. Wu, T. Zhang, G. Compagnini, Z. Feng and A. Hu, *Energ Environ Sci*, 2016, **9**, 1458-1467.
13. C. F. Zhang, M. P. Kremer, A. Seral-Ascaso, S. H. Park, N. McEvoy, B. Anasori, Y. Gogotsi and V. Nicolosi, *Adv Funct Mater*, 2018, **28**.
14. K. Shen, J. Ding and S. Yang, *Adv Energy Mater*, 2018, DOI: 10.1002/aenm.201800408.